Available online at www.sciencedirect.com
ScienceDirect
Journal of Catalysis 251 (2007) 94–102
JOURNAL OF CATALYSIS
www.elsevier.com/locate/jcat

Pd and PdAu on mesoporous silica for methane oxidation: Effect of SO_2

A.M. Venezia [a,*], R. Murania [b], G. Pantaleo [a], G. Deganello [a,b]

[a] *Istituto dei Materiali Nanostrutturati (ISMN-CNR) via Ugo La Malfa, 153, Palermo I-90146, Italy*
[b] *Dipartimento di Chimica Inorganica ed Analitica "Stanislao Cannizzaro", Università di Palermo, Viale delle Scienze – Parco d'Orleans, Palermo I-90128, Italy*

Received 9 May 2007; revised 2 July 2007; accepted 3 July 2007
Available online 27 August 2007

Abstract

Palladium and gold–palladium catalysts supported on mesoporous silica were prepared by incipient wetness impregnation. They were characterized by XPS, XRD, BET, and FTIR acidity measurements. The activity was tested in the oxidation of methane under lean conditions. The effect of adding SO_2 to the reactant mixture was investigated. Test reactions were consecutively performed to evaluate the thermal stability and poisoning reversibility. The palladium catalyst performed quite well in terms of the light-off temperature ($T_{50} < 300\,^{\circ}C$) and SO_2 tolerance. Moreover, the activity, which decreased after a night treatment in SO_2 at 350 °C, was completely recovered in subsequent cycles. The presence of gold decreased the activity slightly without altering the SO_2 tolerance. Evidence of a dynamic reduction–oxidation process occurring at the palladium surface was obtained from the gold-promoted sample in which the reduction of palladium on SO_2 treatment was ascertained.
© 2007 Published by Elsevier Inc.

Keywords: Pd/HMS; Methane oxidation; Gold promotion; SO_2 effect

1. Introduction

Total oxidation of methane is needed in catalytic combustors for power generation, involving high combustion temperatures, and in catalytic converters for lean-burn natural gas-fuelled vehicles (NGVs), typically operating at 320–420 °C [1–3]. With no posttreatment device, the amount of unburned methane released in the atmosphere from lean-burn NGVs exceeds the accepted limits of 1.6 g/kWh in Euro III standards and 1.7 g/kW in US standards [3]. Due to the strong greenhouse effect of this gas, the increasing concerns about environmental pollution demand highly efficient catalysts for the complete abatement of methane emissions. Both classes of catalysts, metal oxides [4–6] and noble metals [2,7] have been and are currently being explored. The noble metal-based catalysts, despite their higher costs, are preferred due to their high specific activity. In particular, those based on supported PdO are among the most active for methane combustion at low temperatures [7,8]. However, as has been pointed out in several studies, their catalytic activity depends strongly on the nature of the support [9], their acidity [7], the palladium precursors [10], and the size of the PdO crystallites. Sintering of the active phase and poisoning by water and sulfur-containing compounds represent major drawbacks [3,9,11]. With respect to the effect of water, the hydrophobicity of the support plays a positive role and accounts for the superior water tolerance of the SiO_2 compared with other oxide supports such as Al_2O_3 and ZrO_2 [12,13]. However, the use of SiO_2 is often considered detrimental because of its only slight interaction with the active site, which gives rise to ready particle agglomeration. To counteract this problem and to take advantage of the large surface area of SiO_2, mesoporous silica with well-controlled pore size structure has been prepared and used as a support for PdO methane oxidation catalysts [14,15]. The advantage of this approach was the improved thermal stability of smaller metal particles with consequent increased activity. The addition of a second noble metal has also been considered as a way to increase the dispersion and thermal stability of the palladium catalysts [16].

In the present work, we compared the catalytic behaviors of Pd and PdAu supported on mesoporous HMS silica in methane oxidation under lean conditions. We also examined the effect of SO_2 both added to the reaction mixture and after overnight exposure under isothermal conditions (350 °C). The choice of

* Corresponding author.
E-mail address: anna@pa.ismn.cnr.it (A.M. Venezia).

0021-9517/$ – see front matter © 2007 Published by Elsevier Inc.
doi:10.1016/j.jcat.2007.07.013

gold as the second metal is dictated by its well-known affinity with sulfur compounds and its ability to alloy with other noble metals [17], aiming to protect palladium from being poisoned and to increase its dispersion. Based on the XPS, SEM, BET, and XRD characterizations, the superior performance of the mesoporous-supported catalyst compared with analogous palladium supported on amorphous SiO_2 is explained in terms of morphological and structural effects.

2. Experimental

2.1. Support and catalyst preparation

The mesostructured HMS material was synthesized as described previously [18]. Basically, HMS was assembled from 4:1 molar mixtures of tetraethyl orthosilicate (TEOS) (Aldrich) as the inorganic precursor and dodecylamine (DDA) (Aldrich) as the structure-directing surfactant in 90:10 (v/v) water/ethanol. About 49 mmol of DDA was dissolved in 50 ml of ethanol and 450 ml of H_2O. To the surfactant solution, heated to 60 °C, 196 mmol of TEOS was added. The gel mixture was kept in a closed Teflon vessel at 60 °C for 20 h. The reaction product was filtered, washed with distilled water, and dried at room temperature for 24 h. The surfactant was removed by calcination in air at 600 °C for 4 h. Attainment of the ordered mesoporous structure was confirmed by the XRD pattern showing a single diffraction line at $2\theta \approx 2°$ and by the typical type IV N_2 adsorption–desorption isotherm [18,19]. The zero point charge (ZPC) at pH 3.9 was obtained using a mass titration method [20].

The catalysts were prepared by incipient wetness impregnation. The monometallic Pd/HMS catalysts were obtained by impregnating the HMS support with an aqueous solution of palladium chloride (Aldrich), followed by drying at 120 °C and calcination at 400 °C for 2 h. The bimetallic PdAu/HMS catalyst was prepared by co-impregnating the HMS with the aqueous solution of the two metal chlorides, $PdCl_2$ (Aldrich) and $AuCl_3$ (Aldrich), followed by the same drying and calcination procedures as described above. For comparison, a Pd catalyst on commercial SiO_2 (amorphous silica gel 60 from Merck, ZPC at pH 6.5) was prepared following the same procedure. In all catalysts, the content of Pd and Au was 1 wt%, as confirmed by XRF spectroscopy.

2.2. Catalyst characterization

XRD patterns were measured using a Philips vertical goniometer using Ni-filtered CuKα radiation with a proportional counter and 0.05° step sizes in 2θ. The assignment of the various crystalline phases was based on the JPDS powder diffraction file cards [21]. From the line broadening of the main reflection peaks, using Scherrer's equation, particle sizes exceeding the detection limit of 3 nm were determined [22].

The microstructural properties of the materials were obtained from N_2 adsorption–desorption isotherms at −196 °C using a Sorptomatic 1900 (Carlo Erba) instrument. Before measurement, the samples were heated in vacuum at 250 °C for 2 h. Specific surface areas and pore size distributions of the materials were obtained using the BET and BJH calculation methods [19].

The FTIR spectra of adsorbed pyridine provided information on the acidity of the two supports, HMS and commercial SiO_2. The spectra were recorded with a Perkin Elmer System 2000 FT-IR spectrophotometer with a resolution of 2 cm^{-1}, as described previously [23]. The reported spectra were subtracted from the spectra of the sample before the admission of pyridine and normalized to the same amount of catalysts per cm^2.

The morphology of the HMS support was examined at different magnifications with a Philips ESEM XL30 scanning electron microscope. The XPS analyses were performed with a VG Microtech ESCA 3000 Multilab, using an unmonochromatized Al$K\alpha$ source (1486.6 eV) run at 14 kV and 15 mA. For the individual peak energy regions, a pass energy of 20 eV was used. Samples were mounted with double-sided adhesive tape. Binding energies were referenced to the C 1s binding energy of adventitious carbon set at 285.1 eV. VG software was used for peak analyses and calculation of atomic concentrations. The precisions on the binding energy and the atomic percentage values were ±0.15 eV and ±10%, respectively.

2.3. Catalytic activity

Methane oxidation catalytic tests were performed using a U-shaped quartz reactor with a inner diameter of 12 mm, electrically heated in a furnace. The catalyst powder (sieved fraction, 180–250 μm) was diluted 1:2 with inert SiC to avoid thermal gradients and was placed on a porous quartz disk. The reaction temperature was measured by a K-type thermocouple in contact with the 12-mm-long catalytic bed. Before catalytic testing, the samples were treated in situ under flowing O_2 (5 vol% in He, 50 ml/min) at 350 °C for 1/2 h and in He during cooling at 200 °C. The standard reagent gas mixture consisting of 0.3 vol% of CH_4 + 2.4 vol% O_2 in He was flowed over the catalyst (50 mg) at a rate of 50 ml/min (STP), equivalent to a weight hourly space velocity (WHSV) of 60 000 ml/(g h). Activity was measured by increasing the temperature from 200 to 600 °C (in steps of 50 °C, hold time 45 min). The inlet and outlet gas compositions were analyzed by on-line mass quadrupole spectroscopy using a Thermostar unit (Balzers) to follow the evolution of CH_4, CO, CO_2, H_2, H_2O, and O_2. Moreover, the concentration of CO and CO_2 species was checked by an IR analyzer (ABB Uras 14), calibrated in the ranges 0–3000 ppm for CO and 0–10,000 ppm for CO_2. The reaction products of methane oxidation were CO_2 and H_2O. No CO was detected in the overall temperature range. The carbon balance was close to ±5% in all of the catalytic tests. Methane oxidation in the presence of SO_2 was determined by co-feeding 10 vol ppm of SO_2. On the samples, overnight treatments were also carried out with flowing 10 vol ppm of SO_2/He and also with 10 vol ppm of SO_2 + 2.4 vol% O_2 in He at 350 °C before the catalytic tests. After consecutive runs were performed, the sample was cooled in inert He atmosphere.

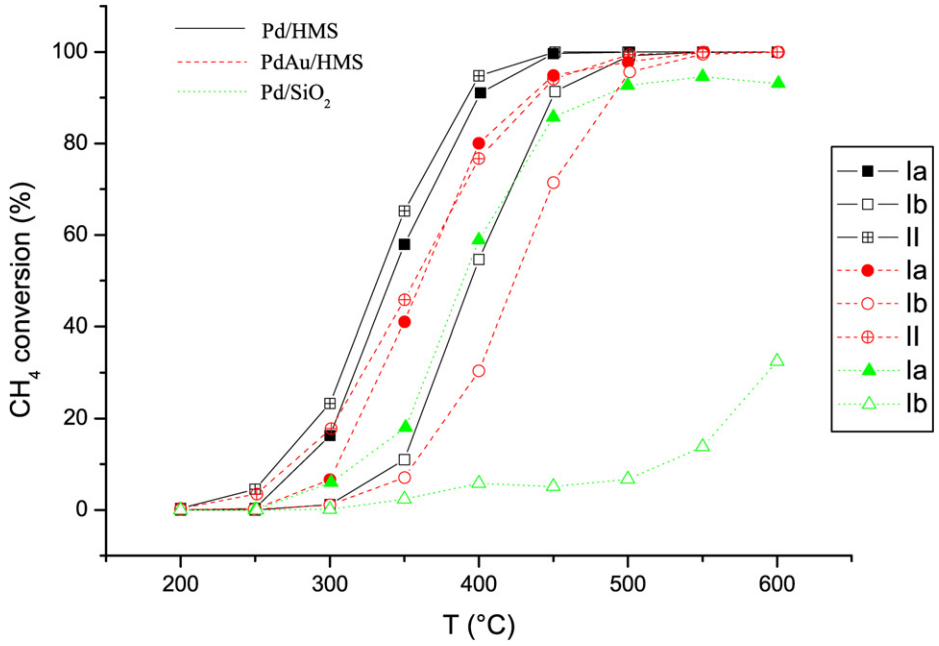

Fig. 1. Methane conversion as a function of reaction temperature: curve Ia (1st run without SO_2); curve Ib (1st run with SO_2); curve II (2nd run without SO_2 after curve Ib).

3. Results and discussion

3.1. Catalytic activity with SO_2-free and SO_2-containing reactant mixtures

Fig. 1 shows the curves of methane conversion as a function of reaction temperature at 200–600 °C over the Pd/HMS and (Pd–Au)/HMS catalysts relative to runs with and without SO_2 in the reagent gas mixture. For comparison, the figure also shows conversion curves relative to the first runs over Pd/SiO_2 with and without SO_2. An initial instability of the catalysts was noted, consisting of increased activity at a given temperature during the time allotted for stabilization (∼45 min). Based on results in the literature [3,24], this enhanced activity during reaction conditions was attributed to the removal of residual chlorine, which, although below the XPS detection limit, acted as an inhibitor. To further confirm this hypothesis, a catalyst prepared from $Pd(NO_3)_2$ precursor exhibited similar steady-state activity but without initial activation. The beneficial effect of the mesoporous support is evident in the conversion curves of the HMS-supported Pd and PdAu catalysts shifted to lower temperature compared with the Pd/SiO_2 catalyst. Relative to the HMS-supported catalysts, according to the curves Ia and Ib of Fig. 1, corresponding to the first runs on fresh catalysts using SO_2- free and SO_2-containing reagent gas mixture, respectively, the methane oxidation reaction was slowed by SO_2 on both catalysts. Such SO_2 poisoning effects are in agreement with several studies performed on PdO over sulfating and non-sulfating supports [11,25,26]. For the catalysts over a sulfating support, like Pd/Al_2O_3, the marked loss of activity was associated with strong adsorption of the SO_3 arising from the oxidation of SO_2, requiring rather complex regeneration procedures [11,26]. In contrast, the performance of these catalysts on HMS was completely restored and even improved in the subsequent SO_2-free run (curves II). Easy regeneration of an SO_2-poisoned silica-supported Pd catalyst by flowing of the reactant mixture has been reported and attributed to thermal desorption of the sulfate groups from the palladium particles [2,25]. However, it is worth noting that deactivation of the HMS catalysts in the presence of SO_2 disappears at 450 °C, below the temperature at which the decomposition of $PdSO_4$ occurs [3]. For the Pd/SiO_2 sample, the missing full conversion, the deactivation associated with the high-temperature decline of the conversion curve of the SO_2-free run, and the substantial loss of activity demonstrated in the presence of SO_2 discouraged us from continuing any additional tests on this sample.

To evaluate the changes and the tolerance of the catalyst during a more drastic exposure to SO_2, an isothermal treatment at 350 °C in flowing He with 10 ppm SO_2 was carried out overnight (after the run corresponding to curve II of Fig. 1). The catalytic behavior of the Pd and PdAu catalysts after this treatment is shown in Fig. 2. In the run performed in the absence of SO_2 (corresponding to a third run, after the run represented by curve II of Fig. 1) described by curve III, a decrease in activity occurred. Then, in the subsequent run (curve IV), complete recovery with even significantly improved activity was observed. To get information on the active site variation due to the promoter (Au) and/or SO_2 poisoning, the apparent activation energies were determined. Given the high conversion levels of methane, the integral equation of a first-order reaction with respect to methane and pseudo-zero order with respect to oxygen was used for calculating the reaction rate constants k [8,25]. Concerning the effect of water, although water is known to affect the catalyst performance, an order of -1 for water concentration, widely proposed in the literature, leads to overestimation of the effect. Consequently, a smaller value

of −0.25 was recently reported for Pd/SiO_2 [12]. In addition, it was shown that the water formed in the reaction deactivated the catalyst only slightly, with effects becoming noticeable only when a large amount (>20.000 ppm) of water was added [27]. Considering the limited amount of water generated under the present conditions, its inhibiting effect can be neglected here.

For some selected runs, the activation energies E_{act} and the pre-exponential factor A of the Arrhenius law, $k = A\exp(-E_{act}/RT)$, were calculated from the Arrhenius plot of ln(k) versus 1/T in the temperature range of 300–400 °C (Fig. 3). Table 1 reports the catalytic results in terms of temperatures of half conversion (T_{50}), apparent activation energies, and pre-exponential factors. Over the monometallic catalysts Pd/SiO_2 and Pd/HMS, the activation energies for the runs without SO_2 were comparable with values previously reported for methane oxidation over Pd/SiO_2 and Pd/ZrO_2 [25,28]. As shown in Fig. 3 and Table 1, larger E_{act} values and larger pre-exponential factors were obtained with the sulfur-containing reactant mixture. Then in the subsequent run, as shown for the Pd/HMS catalyst, the activation energy decreased, suggesting reactivation of the catalyst by the simple reactant mixture. An analogous behavior was obtained with the bimetallic PdAu/HMS catalyst, but with larger activation energies. Sim-

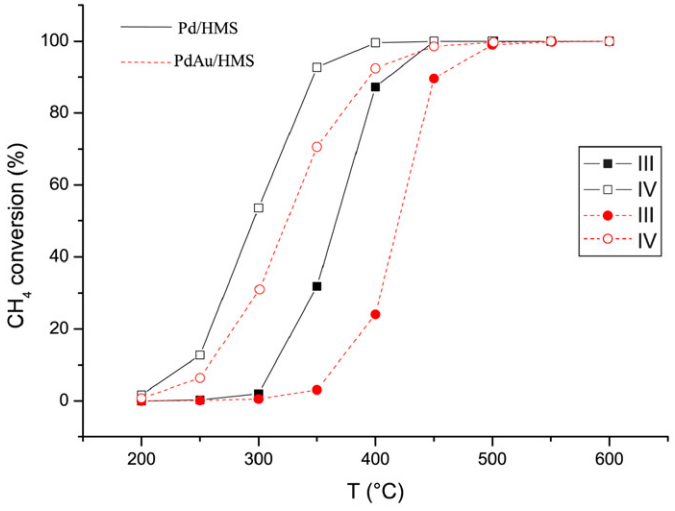

Fig. 2. Methane conversion on Pd/HMS and PdAu/HMS as a function of reaction temperature. Curve III (3rd run without SO_2 after curve II and overnight treatment in SO_2); Curve IV (4th run without SO_2 after curve III).

Table 1
Kinetic data for the Pd/HMS catalyst after different runs.[a] The corresponding data relative to a first run without and with SO_2 over Pd/SiO_2 are also listed

Samples	T_{50} (°C)	E_{act} (kJ/mol)	ln A[b]
Pd/SiO_2			
SO_2-free run	390	86	18
1st run with SO_2	>600	133	24
Pd/HMS			
SO_2-free run	341	83	19
1st run with SO_2	394	135	27
2nd run SO_2-free	332	50	13
3rd run SO_2-free after pretreat SO_2	366	148	30
4th SO_2-free run	296	60	16
PdAu/HMS			
SO_2-free run	360	101	22
1st run with SO_2	424	112	24
2nd run SO_2-free	356	65	15
3rd run SO_2-free after pretreat SO_2	418	127	24
4th SO_2-free run	328	56	15

[a] T_{50} is the temperature at which the 50% of methane has been converted; E_{act} and A are the apparent activation energy and the pre-exponential factor respectively calculated from the Arrhenius plot in the temperature range 300–400 °C.
[b] The error in the determination of this parameter, as obtained from the linear least squares fitting of the Arrhenius curve is ⩽10%.

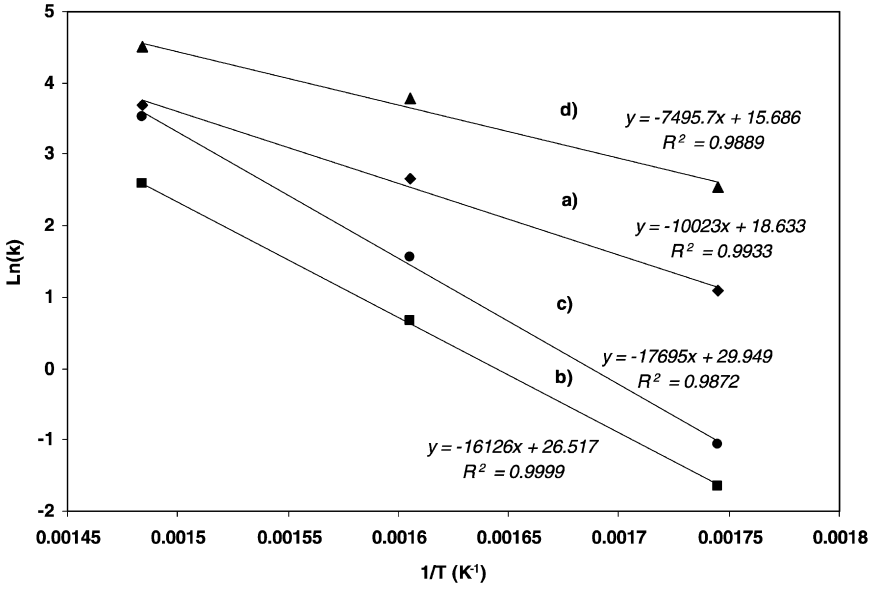

Fig. 3. Arrhenius plots for the methane conversion on Pd/HMS. (a) 1st run SO_2-free; (b) 1st run with SO_2; (c) 3rd run after overnight treatment in SO_2; (d) 4th run SO_2-free.

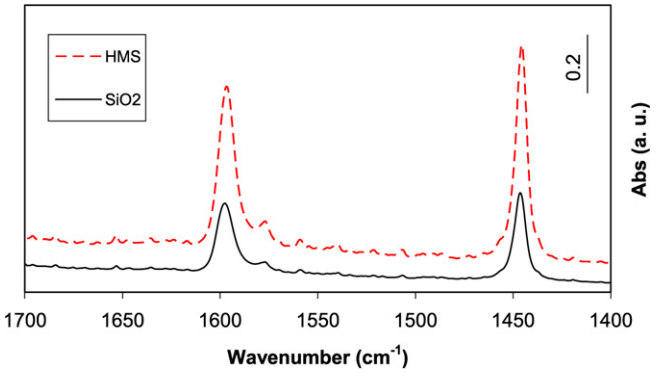

Fig. 4. FT-IR spectra of adsorbed pyridine on HMS and commercial SiO_2.

ilar trends were obtained for the runs after the SO_2 overnight treatment and the subsequent fourth run.

Our results can be summarized as follows:

1. The Pd/HMS-supported catalyst exhibited better activity in terms of ignition temperature (T_{50}) and total conversion temperature compared with the SiO_2-supported catalyst and also compared with some recent literature results on other mesoporous silica-supported Pd catalysts [13,14].
2. SO_2 in the reactant mixture deactivated Pd/HMS and Pd–Au/HMS. The complete disappearance of the poisoning effect in the subsequent SO_2-free run was accompanied by a slight increase in activity ($\Delta T_{50} = -9$ and $-4\,^{\circ}C$ for the two catalysts).
3. Overnight isothermal treatment in SO_2 at 350 °C followed by a SO_2-free run found a noticeable increase in the activity ($\Delta T_{50} = -45$ and $-32\,^{\circ}C$ for the monometallic and bimetallic catalysts, respectively). According to the Arrhenius parameters (E_{act} and A), modification of the active sites with enhanced intrinsic activity occurred.
4. The presence of gold modified the active sites, reducing their intrinsic activity, in accordance with a larger E_{act}, but slightly increasing their numbers, as deduced from the A factor.

3.2. Characterization of fresh and treated catalysts

To find the reason for the different catalytic behavior of the palladium supported on the commercial and mesoporous silica samples, the supports were characterized by different experimental techniques. Their surface acidity was determined by IR spectroscopy of the adsorbed pyridine. The FTIR spectra of the investigated silicas after adsorption of pyridine and outgassing at room temperature are shown in Fig. 4. The spectra exhibited two main bands at 1447 and 1599 cm^{-1}. According to the literature [29,30], these bands can be attributed respectively to the 8a and 19b modes of pyridine molecules interacting via H bonding with the acidic surface hydroxyl groups (silanols) of silicas. But the shifts of both bands with respect to those of not-bonded pyridine were not sufficiently large to indicate Lewis acidity; both bands were also completely pumped off at 150 °C. Moreover, the absence of a band at 1540 cm^{-1} indicated that silanol groups, being rather weak, were not able to protonate pyridine.

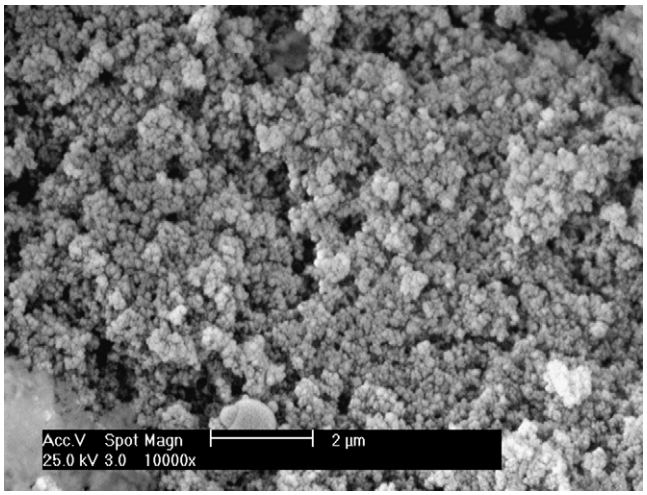

Fig. 5. SEM micrograph of HMS support.

Table 2
BET surface area (SSA), pore size (D) and crystal size (d) of support and catalyst materials

Sample[b]	SSA (m^2/g)	D (nm)	d_{PdO}[a] (nm)	d_{Au} (nm)	$d_{Au_{45}Pd_{55}}$ (nm)
HMS	790	3.4			
Pd/HMS *fresh*	650	3.6	3.5 (59%) 9.0 (41%)	–	–
Pd/HMS *spent*	–	–	3.1 (67%) 9.6 (33%)	–	–
PdAu/HMS *fresh*	668	3.6	7.0	18	–
PdAu/HMS *spent*	–	–	4.0	–	9
SiO_2	316	5.0	–	–	–
Pd/SiO_2	270	5.0	7	–	–
Pd/SiO_2 spent[c]	–		5		

[a] The values in parentheses represent the relative percentage of particles as obtained from PdO(101) peak fitting.

[b] *Fresh* and *spent* indicates the catalysts after calcination and after the 4th run as in Table 1, respectively.

[c] This catalyst underwent 1 run with SO_2 in the reactant mixture.

Comparing the spectra of the two silica demonstrated a clear difference in the intensity of the pyridine bands, with HMS exhibiting stronger bands compared with commercial SiO_2. No significant difference in the frequency of the bands was observed, however. This behavior suggests that the two silicas differed in terms of number of acid sites (silanol groups) but not in terms of acid strength. Such difference could partially account for the better dispersion of the PdO crystallites over the HMS support.

The spongy morphology of the HMS support was evidenced by the SEM image shown in Fig. 5. The specific surface area and the pore sizes of the supports and corresponding catalysts, along with the PdO and Au particle diameters, from XRD measurements are listed in Table 2. The HMS was characterized by a much larger surface area and smaller pore size compared with the amorphous SiO_2 support. On deposition of the metal, the support surface area decreased by about 17%. Smaller PdO particle sizes were detected with the mesoporous support. The particle sizes of the catalysts analyzed after the fourth run, described by the curves IV in Fig. 2, indicated as "spent," are also

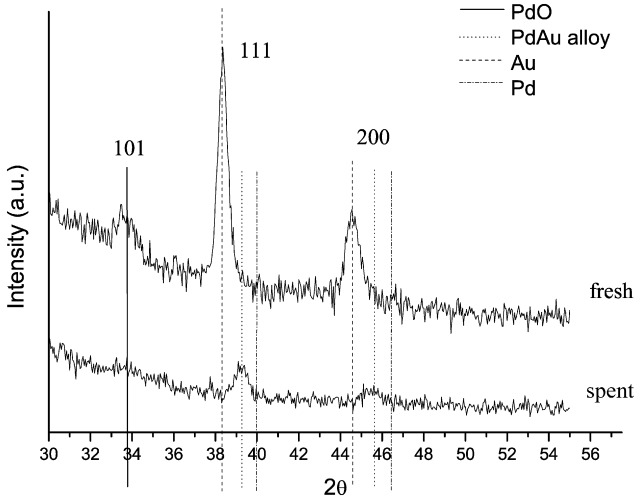

Fig. 6. XRD patterns of PdAu/HMS fresh and spent (4th cycle including overnight treatment in SO_2).

given. Curve-fitting the PdO(101) peak ($2\theta \sim 34°$) of the fresh and spent Pd/HMS catalysts with two components yielded PdO particles of ∼3 and ∼9 nm with relative percentages as given in Table 2. It is noteworthy that whereas the sizes obtained for the fresh and spent catalysts were similar, the relative ratio of the small to large particles was larger in the spent catalyst. In PdAu/HMS and Pd/SiO_2, only particles of one dimension (smaller in the spent catalysts) were obtained. The XRD patterns of the fresh and spent PdAu/HMS catalysts are given in Fig. 6. The fresh catalyst is characterized by 7-nm PdO particles and large (18-nm) Au particles. Different from the spent Pd/HMS catalyst, which exhibited smaller PdO crystallite sizes, quite drastic modification of the catalyst structures was detected in the spent bimetallic PdAu/HMS. Indeed, along with some detectable 4-nm PdO crystallites, new diffraction peaks attributable to an alloy phase, $Au_{45}Pd_{55}$, as derived from the 2θ shift [17], were observed with the complete disappearance of the Au-related peaks. As derived from the Scherrer analysis of the peaks, alloy particles of ∼9 nm were identified.

Information on the chemical state and the surface composition of the catalysts before and after the catalytic tests were obtained by XPS analyses. Table 3 summarizes the Pd $3d_{5/2}$ and Au $4f_{7/2}$ binding energies and the Pd/Si and Au/Si surface atomic ratios. The overlapping of a very weak Au $4d_{3/2}$ component was neglected in the fitting procedure of the Pd 3d. Note that despite the smaller surface area of the SiO_2 support, a lower Pd/Si atomic ratio was obtained for the amorphous silica catalyst compared with the HMS ones, in accordance with the slightly larger average PdO particle size detected by XRD as well as some hidden particles inside the larger pores of the amorphous silica. This atomic ratio decreased after the subsequent treatments in all of the catalysts, but to the greatest extent in Pd/SiO_2. This decrease was independent of the presence of SO_2 and also in contradiction with the smaller particle sizes detected by XRD on the used catalysts. In this case, a thermal-driven inward diffusion of palladium rather than SO_2-driven sintering may have accounted for the atomic ratio variations. In contrast, the Au/Si atomic ratio increased, in accordance with

Table 3
XPS binding energies (eV) and surface atomic ratios of the catalysts after different stages. FWHM (eV) are given in parentheses

Sample	Pd $3d_{5/2}$	Au $4f_{7/2}$	S 2p	Pd/Si	Au/Si
Pd/SiO_2					
Fresh	337.8 (2.5)	–		0.003	
1st run SO_2-free	337.6 (2.4)		–	0.001	
15 h SO_2[a]	337.7 (3.0)		170.4 (4.0)[b]	0.001	
Pd/HMS					
fresh	337.6 (3.1)	–		0.005	–
1st run SO_2-free	337.6 (2.8)			0.004	
4th SO_2-free run	337.5 (2.9)	–		0.004	–
15 h SO_2[a]	337.3 (3.2)		170.4 (4.0)[b]	0.004	
15 h $SO_2 + O_2$[c]	337.4 (3.6)		170.3 (2.6)[b]	0.004	
PdAu/HMS					
Fresh	337.8 (3.4)	85.1 (0.9)		0.005	0.001
3rd run SO_2-free after pretreat SO_2	335.1 (2.5)	85.1 (1.9)		0.004	0.002
	336.1 (2.5	83.5 (1.9)			
	337.9 (2.5)				
4th SO_2-free run	336.7 (4.2)	84.8 (1.8)	–	0.004	0.002

[a] The XPS measurement after overnight treatment in 10 vol ppm SO_2 at 350 °C.
[b] In the ultra high vacuum the S 2p signal decreased with time until its complete disappearance.
[c] The XPS measurement after overnight with 10 vol ppm SO_2 and 2.4 vol% O_2 in He at 350 °C.

the smaller alloy particle sizes detected by XRD. The binding energy of Pd $3d_{5/2}$ in the fresh catalysts was 337.8 ± 0.1 eV; this could be assigned to highly oxidized palladium Pd^{4+} as in PdO_2 [31,32]. Although this oxide is rather unstable at high temperatures, it was found with different supports [16,17,32]. Its formation was attributed to calcination in air, during which the oxygen species were incorporated into the PdO crystal lattice [32]. However, considering that it was not detected by XRD, PdO_2 had to be present only at the surface of the catalyst. As

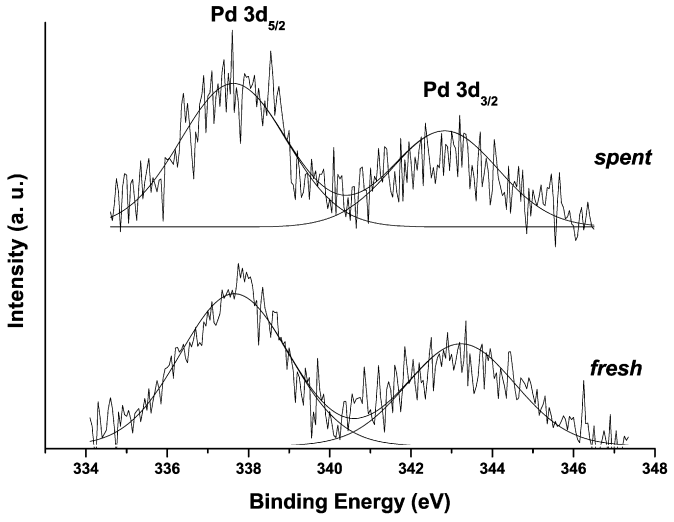

Fig. 7. Pd 3d spectra of Pd/HMS fresh and spent (4th cycle including overnight treatment in SO_2).

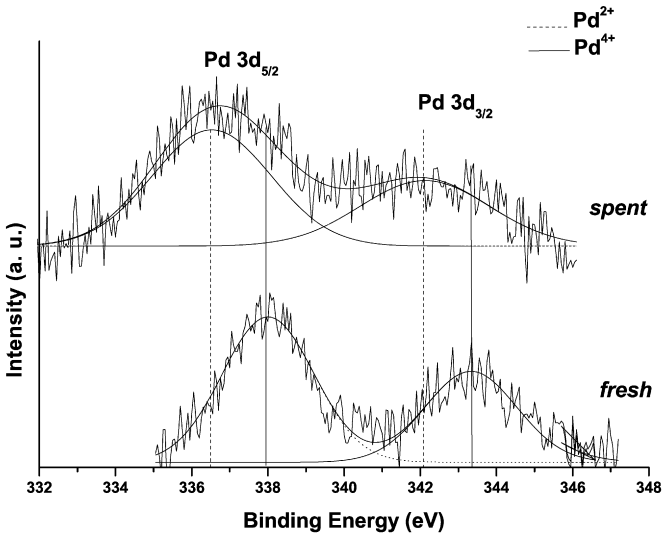

Fig. 8. Pd 3d spectra of PdAu/HMS fresh and spent (4th cycle including overnight treatment in SO_2).

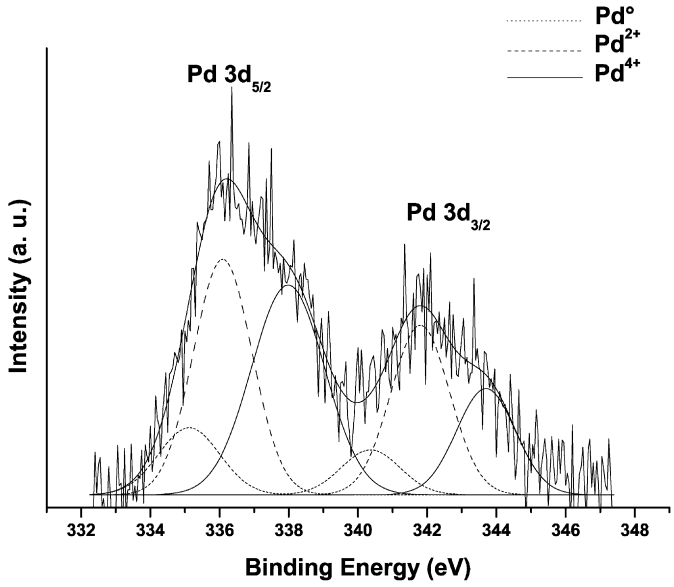

Fig. 9. Pd 3d XP spectra of PdAu/HMS after the 3rd run (including the overnight SO_2 treatment).

shown in Table 3, no changes in the Pd 3d binding energy of the Pd/SiO_2 and Pd/HMS occurred after the first run without SO_2. Considering the XPS results obtained after the SO_2 treatment and the two catalytic tests (i.e., after the fourth SO_2-free run), as shown in Table 3 and Figs. 7 and 8, the Pd 3d binding energy of PdAu/HMS shifted toward lower energy, different than the monometallic catalyst. Moreover, aiming to find the explanation for the increased activity in the fourth run, the bimetallic sample was analyzed by XPS also after the third run. Curve fitting of the corresponding Pd 3d spectrum allowed discrimination of three components, as shown in Fig. 9. The low-energy component at 335.1 eV was due to metallic Pd, which, according to XRD, was alloyed with Au. The component at 336.1 eV was due to PdO, and the high-energy component at 337.9 eV was attributed to Pd^{4+}. These data confirm that in the presence of SO_2, reduction of palladium occurred, in accordance also with the chemical shift observed after the fourth run, and gold enabled the detection of this process by alloying with palladium. Accordingly, the reducing action of SO_2 over PdO or PdO_2, which was just speculated to occur on the monometallic catalyst, was in fact confirmed in the bimetallic system, due to the gold property of capturing and stabilizing the reduced palladium. Interestingly, analysis of the samples after the catalytic tests performed with SO_2 added to the reactant mixture revealed no S 2p signal. To further investigate the formation of sulfate species, generally considered responsible for PdO catalyst deactivation [11,25,26], XPS analyses of samples after a long treatment (15 h) with SO_2 at 350 °C with and without O_2 were performed. The corresponding data are given in Table 3. Regardless of the type of silica used, no significant Pd 3d binding energy shift occurred. A broad S 2p at 170.4 eV characteristic of SO_x species was found on Pd/SiO_2 and Pd/HMS after SO_2 treatment without and with oxygen. The intensity of the signal decreased strongly with the time that the sample spent in the ultra-high-vacuum system. The finding that the appearance of SO_x species was not accompanied by a shift in the Pd 3d at the higher binding energy typical of $PdSO_4$ excluded the formation of a well-defined palladium sulfate. Moreover, in the absence of oxygen, SO_2 could oxidize to SO_3 by reducing PdO to Pd^0 [11]. Nevertheless, the lack of XPS and XRD evidence of metallic Pd, along with the broad (FWHM = 4 eV) and labile S 2p signal, were indicative of a mixture of SO_2–SO_3 weakly chemisorbed on the oxidized Pd. In the presence of oxygen, SO_2 is readily oxidized to SO_3, thereby producing a narrower S 2p signal. The partly reduced palladium, tracked only in the bimetallic catalyst, is easily reoxidized to PdO on which the SO_3 is weakly bound, as suggested again by the easy removal under vacuum.

To summarize, the better activity of the HMS-supported Pd catalyst compared with the SiO_2 catalyst can be attributed to the better PdO dispersion and the stronger resistance to sintering, as determined by XRD and XPS. Such properties are likely associated with the nature of the support, characterized by a regular mesoporous structure acting to confine the supported particles and by a larger number of acidic surface hydroxyl-groups as detected by IR spectroscopy. Moreover, in accordance with the literature and with the nonsulfating nature of silica, the presence of SO_2 during methane oxidation has a twofold effect, reducing PdO to the less-active metallic Pd and chemisorbing on the active PdO site, forming a new palladium-containing species that is less effective for C–H activation [33]. However, compared with palladium on commercial SiO_2, for which drastic deactivation occurred, a much better tolerance to the SO_2 was found for the Pd/HMS and PdAu/HMS catalysts. Given the dual distribution of PdO particle sizes, it is reasonable to suppose that the larger particles lying outside the pores are most affected by the SO_2, and thus the smaller particles localized inside the mesoporous channels are more protected and therefore maintain their activity. Based on the properties of the gold-promoted catalysts, the reduction of palladium during methane oxidation in the presence of SO_2 under an excess of oxygen was ascertained. The rearrangement of the bimodal distribution of PdO

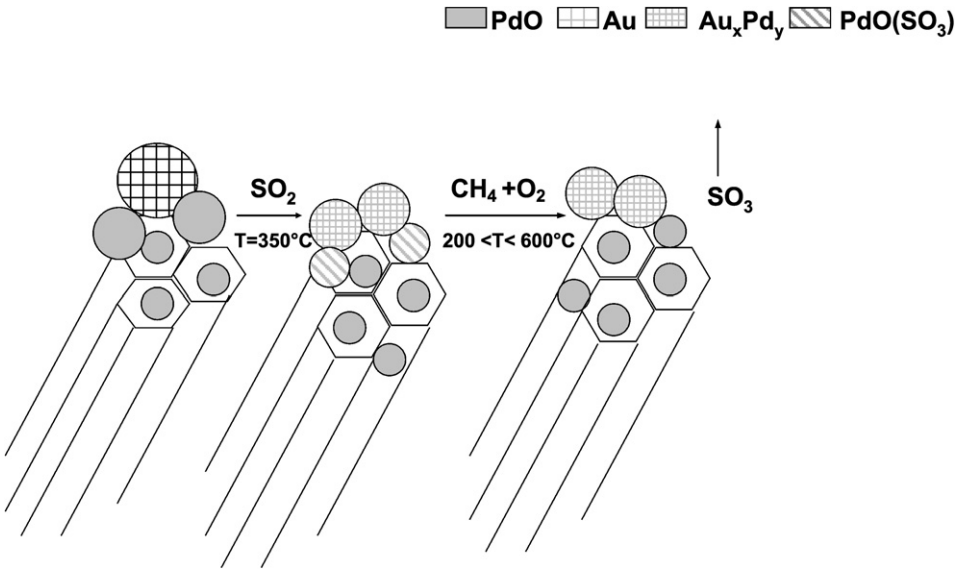

Fig. 10. Schematic of possible mechanism of action of SO_2 and the following reaction mixture on the PdAu/HMS catalyst.

with an increased number of smaller particles compared with larger particles, as evidenced in the bimetallic catalyst by the sequestration of Pd^0 alloyed by Au, may explain the increased catalyst activity after treatment in SO_2 followed by a test in SO_2-free reactant mixture. In other words, the treatment with SO_2, through a dynamic equilibrium between a reduced and an oxidized state of palladium, is responsible for the increased PdO dispersion and the consequent increased activity in both the monometallic and bimetallic catalysts. Such a process is schematically illustrated in Fig. 10 for the bimetallic PdAu catalyst and can be extended to the monometallic Pd/HMS, where the reoxidation of palladium probably occurred too rapidly to be detected by XPS and XRD.

4. Conclusion

A much better-performing PdO catalyst in methane oxidation was obtained on HMS compared with commercial SiO_2. The Pd/HMS catalyst indeed exhibited higher activity at low temperatures ($T_{50} \sim 300\,^{\circ}C$ and $T_{100} \leqslant 500\,^{\circ}C$) and good tolerance to the SO_2 present in the reagent mixture. Due to the support morphology, a bimodal distribution of particles was obtained on the HMS. As suggested by the limited loss of activity in the presence of SO_2, this molecule was likely to interact more with the larger particles, by reducing some of them and forming a composite species of lower activity, like PdO–SO_3, in accordance with the increase in activation energy. This composite was labile and easily decomposed at $T \geqslant 450\,^{\circ}C$. The complete recovery with a distinct enhancement of the catalytic activity by subsequent runs with the reagent gas mixture demonstrates that these systems are quite promising for the abatement of unburned CH_4 in NGVs.

Acknowledgments

Financial support was provided by the European Community, Network of Excellence (NoE) IDECAT (Integrated Design of Catalytic Nanomaterials for Sustainable Production) and COST D36 action.

References

[1] R.A. Betta, Catal. Today 35 (1997) 129.
[2] J.K. Lambert, M.S. Kazi, R. Farrauto, J. Appl. Catal. 14 (1997) 211.
[3] P. Gelin, M. Primet, Appl. Catal. B 39 (2002) 1.
[4] L.F. Liotta, G. Di Carlo, G. Pantaleo, A.M. Venezia, G. Deganello, Appl. Catal. B 66 (2006) 217.
[5] N. Bahlawane, Appl. Catal. B 67 (2006) 168.
[6] T.V. Choudhary, S. Banerjeem, V.R. Choudhary, Appl. Catal. A 234 (2002) 1.
[7] H. Yoshida, T. Nakajima, Y. Yazawa, T. Hattori, Appl. Catal. B 71 (2007) 70.
[8] K. Fujimoto, F.H. Ribeiro, M.A. Borja, E. Iglesia, J. Catal. 179 (1998) 431.
[9] M. Shmal, M.M.V.M. Souza, V.V. Alegre, M.A. Pereira da Silva, D.V. Cesar, C.A.C. Perez, Catal. Today 118 (2006) 392.
[10] L.M.T. Simplicio, S.T. Brandao, E.A. Sales, L. Lietti, F. Bozon-Verduraz, Appl. Catal. B 63 (2006) 9.
[11] D.L. Mowery, R.L. McCormick, Appl. Catal. B 34 (2001) 287.
[12] P. Araya, S. Guerrero, J. Robertson, F.J. Garcia, Appl. Catal. A 283 (2005) 225.
[13] K. Okumura, E. Shinohara, M. Niwa, Catal. Today 117 (2006) 577.
[14] I. Yuranov, P. Moeckli, E. Suvorova, P. Buffat, L. Kiwi-Minsker, A. Renken, J. Mol. Catal. A 192 (2003) 239.
[15] G. Pecchi, P. Reyes, I. Concha, J.L.G. Fierro, J. Catal. 179 (1998) 309.
[16] K. Persson, K. Jansson, S.G. Jaras, J. Catal. 245 (2007) 401.
[17] A.M. Venezia, V. La Parola, V. Nicolì, G. Deganello, J. Catal. 212 (2002) 5.
[18] N. Marin-Astorga, G. Pecchi, T.J. Pinnavaia, G. Alvez-Manoli, P. Reyes, J. Mol. Catal. A 247 (2006) 145.
[19] S.J. Gregg, K.S. Sing, Adsorption, Surface Area and Porosity, second ed., Academic Press, San Diego, 1982.
[20] S. Subramanian, J.S. Noh, J.A. Schwarz, J. Catal. 114 (1988) 433.
[21] JCPDS Powder Diffraction File, Int. Centre for Diffraction Data, Swarthmore.
[22] H.P. Klug, X-Ray Diffraction Procedure for Polycrystalline and Amorphous Materials, Wiley, New York, 1954.
[23] V. La Parola, G. Deganello, S. Scirè, A.M. Venezia, Solid State Chem. 174 (2003) 482.
[24] D. Roth, P. Gelin, M. Primet, E. Tena, Appl. Catal. 203 (2000) 37.

[25] L.J. Hoyos, H. Praliaud, M. Primet, Appl. Catal. A 98 (1993) 125.
[26] F. Arosio, S. Colussi, G. Groppi, A. Trovarelli, Catal. Today 117 (2006) 569.
[27] P. Hurtado, S. Ordonez, H. Sastre, F.V. Diez, Appl. Catal. B 47 (2004) 85.
[28] F.H. Ribeiro, M. Chow, R.A. Dalla Betta, J. Catal. 146 (1994) 537.
[29] E.P. Parry, J. Catal. 2 (1963) 371.
[30] G. Busca, Catal. Today 41 (1998) 191.
[31] D.H. Kim, S.I. Woo, J.M. Lee, O.B. Yang, Catal. Lett. 70 (2000) 35.
[32] Y. Bi, G. Lu, Appl. Catal. B 41 (2003) 279.
[33] R. Burch, D.J. Crittle, M.J. Hayes, Catal. Today 47 (1999) 229.